Acta Pharmaceutica Sinica B 2026;16(2):1155−1165

Chinese Pharmaceutical Association
Institute of Materia Medica, Chinese Academy of Medical Sciences

Acta Pharmaceutica Sinica B

www.elsevier.com/locate/apsb
www.sciencedirect.com

SHORT COMMUNICATION

Rapid *in vivo* release of paclitaxel from polymeric micelles

Haisheng He[a], Jianping Qi[a], Yi Lu[a,c,d], Wei Wu[a,b,c,d,*]

[a]*School of Pharmaceutical Sciences, Fudan University, Key Laboratory of Smart Drug Delivery of MOE and National Key Laboratory of Advanced Drug Formulations for Overcoming Delivery Barriers, Shanghai 201203, China*
[b]*Center for Medical Research and Innovation, Shanghai Pudong Hospital, Fudan University Pudong Medical Center, Shanghai 201399, China*
[c]*Shanghai Engineering Research Center of Topical Chinese Medicine and Shanghai Skin Disease Hospital, Tongji University School of Medicine, Shanghai 200443, China*
[d]*Fudan Zhangjiang Institute, Shanghai 201203, China*

Received 1 September 2025; received in revised form 3 November 2025; accepted 11 November 2025

KEY WORDS

Polymeric micelles;
mPEG-PDLLA;
Paclitaxel;
Drug delivery;
In vivo release;
In vivo fate;
Particokinetics;
Pharmacokinetics

Abstract Profiling *in vivo* release kinetics of drug nanocarriers is of high translational significance. However, this has remained unrealized due to the lack of direct methodologies to quantify either the total released or residual drugs. This study employed an indirect strategy, comparing pharmacokinetics and particokinetics, to estimate the *in vivo* release kinetics of paclitaxel (PTX) from intravenously administered mPEG-PDLLA polymeric micelles (PMs). Blood pharmacokinetics were profiled by chromatographically quantifying PTX, while particokinetics were determined following labeling PM particles by near-infrared fluorophores with aggregation-caused quenching properties. By monitoring the dynamic change in the PTX-to-copolymer ratio, the *in vivo* release of PTX from the PMs was estimated. The results revealed surprisingly rapid release, with over 88.2% and 99.0% of PTX released by 15 s and 5 min post-administration, respectively. It is concluded that PTX is released rapidly from PMs *in vivo*, and PMs may merely work as "solvents" to solubilize PTX rather than as carriers for targeted delivery.

*Corresponding author.
E-mail address: wuwei@shmu.edu.cn (Wei Wu).

Peer review under the responsibility of Chinese Pharmaceutical Association and Institute of Materia Medica, Chinese Academy of Medical Sciences.

https://doi.org/10.1016/j.apsb.2025.11.034

1. Introduction

Polymeric micelles (PMs) are "core/shell" nanostructures, comprising a hydrophobic core and hydrophilic shell, spontaneously assembled from amphiphilic copolymers in aqueous environments through micellization[1,2]. PMs demonstrate significant potential as nanocarriers for drug delivery due to their capacity to solubilize highly hydrophobic payloads[3-8]. Compared to micelles formed by small-molecule surfactants, PMs offer distinct advantages. The extended copolymer chains confer enhanced structural stability and provide larger core volumes for drug encapsulation[2,9-11]. Furthermore, PMs exhibit critical micelle concentrations (CMCs) typically in the micromolar or even nanomolar range[1,3,7], substantially lower than the millimolar CMCs characteristic of small-molecule surfactants (SMS). Consequently, PMs can maintain structural integrity in biological environments, as relatively low copolymer concentrations suffice to exceed the CMC[12-14].

Paclitaxel (PTX), a broad-spectrum anticancer taxane, suffers from extremely poor aqueous solubility[15]. Its original injectable formulation (Taxol®) contained 6 mg PTX solubilized in a vehicle of Cremophor EL® (polyoxyethylated castor oil, 527 mg) and ethanol (49.7%, *v/v*)[16-18]. However, Cremophor EL® induces significant toxicities, including hypersensitivity reactions, necessitating premedication with antihistamines, H_2 antagonists, and corticosteroids[17]. To circumvent these issues, Cremophor-free PTX delivery systems—including liposomes, albumin nanoparticles, and PMs—have been developed[16-18]. A specific PTX-PM formulation, based on methoxy poly(ethylene glycol)-poly(D,L-lactide) (mPEG-PDLLA) copolymer self-assembly[17,18], was first marketed in South Korea (Genexol-PM®) and then in China (Zisun®) and is currently in various stages of global clinical trials[14,19].

PMs achieve prolonged circulation times, enabling passive targeting to tissues beyond the mononuclear phagocyte system (MPS), particularly tumors, *via* the enhanced permeation and retention effect[20,21]. Effective PTX delivery by PMs presupposes minimal premature drug leakage en route to target sites[22,23]. Secure encapsulation, persisting at least throughout systemic circulation, is essential for efficient delivery. Conversely, rapid PTX release upon entering the bloodstream would imply that PMs function merely as "solvents", unloading free drug rapidly while only "empty" micelles reach the target. Previous studies on PTX release from polymeric nanoparticles[24] and *in vitro* PM stability[25] hinted at potential premature leakage, but conclusive *in vivo* evidence has been lacking. Therefore, elucidating the *in vivo* release behavior of PTX from PMs is critically important for understanding their true role and translational potential.

Quantifying drug release from carrier systems typically involves measuring either released or residual (encapsulated) drug after separation. While readily achievable *in vitro* using specialized apparatus, this approach is impractical for multi-unit nanocarrier systems *in vivo* due to the infeasibility of real-time nanocarrier/drug separation. Consequently, methodologies for profiling *in vivo* drug release kinetics remain unavailable.

This proof-of-concept study introduces a novel strategy to estimate *in vivo* PTX release from model mPEG-PDLLA PMs by comparing PTX pharmacokinetics with PM particokinetics. The results reveal a significant divergence between the PTX pharmacokinetic profile and the PM particokinetic profile, indicating rapid dissociation of PTX from the micellar carriers following intravenous administration. By dynamically monitoring the PTX-to-copolymer mass ratio, *in vivo* PTX release profiles from the PMs were generated.

2. Materials and methods

2.1. Materials

PTX and docetaxel (DTX) were supplied by Meilun Biology Technology Co., Ltd. (Dalian, China). The ACQ dye P2 was synthesized as previously reported[26]. Taxol® was purchased from Corden Pharma Latina S.P.A. (Latina, Italy). Methoxy poly-ethylene glycol-poly (D,L-lactide) ($mPEG_{2k}$-$PDLLA_{2.5k}$) was kindly supplied by Prof. Zhiyong Qian at Sichuan University, Chengdu, China. Dichloromethane and acetonitrile were purchased from Sinopharm Chemical Reagent Co., Ltd. (Shanghai, China). Deionized water was obtained by a Milli-Q purification system (Molsheim, France). All other reagents used in this study were of analytical grade and used as received. The Sprague−Dawley (SD) rats were supplied by Shanghai Laboratory Animal Center (Shanghai, China) and raised in the Laboratory Animal Holding Building of the School of Pharmacy, Fudan University (Shanghai, China). Throughout the experiment, the animals were housed at a temperature of 25 ± 1 °C, relative humidity of 55 ± 5%, and with 12 h light-dark cycles. All animal care and experimental procedures were conducted following the guidelines issued by the Ethical Committee of the School of Pharmacy (Protocol approval number: 2021-03-YJ-HHS-29), Fudan University on the use of experimental animals, as well as the principles outlined in the Declaration of Helsinki for all human and animal experimental investigations.

2.2. Preparation of fluorescently labeled PTX-loaded mPEG-PDLLA PMs

mPEG-PDLLA PMs coloaded with P2 and PTX were prepared according to our previous procedures with minor modifications[7,27]. Briefly, accurate amounts of mPEG-PDLLA, PTX, and P2 (1600:160:1, *w/w/w*) were weighed and dissolved in 5 mL of acetonitrile. After complete evaporation of acetonitrile at 50 °C and 10 Pa, the obtained thin film was hydrated by prewarmed saline under mild stirring (60 rpm, HB10 rotary evaporator, IKA, Germany) at 50 °C for 2 min. Unencapsulated PTX was removed by filtration with a 0.22 μm filter. The dispersion was stored at 4 °C before use.

2.3. Preparation of fluorescently labeled commercial Taxol

P2 (80 μg) was dissolved in 2 mL dichloromethane and added to a brown vial. The solvent was completely evaporated under nitrogen; afterwards, 2 mL of Taxol was added into the vial to encapsulate P2 under mild stirring (500 rpm, RCT basic thermostatic magnetic stirrer, IKA, Germany) for 4 h and subsequently stored at 4 °C. Before use, P2-loaded Taxol was diluted 8-fold with saline and filtered through a 0.22 μm filter.

2.4. Characterization of polymeric micelles and Taxol micelles

The average particle size, size distribution, and zeta potential of the PMs were determined by dynamic light scattering (DLS) using a Zetasizer Nano (Malvern Instruments, Malvern, UK) equipped with a 4 mW He−Ne laser at 633 nm under ambient temperature. All measurements were performed with a scattering angle of 173° at 25 °C after diluting the micellar solution to an appropriate volume with deionized water. The morphologies of mPEG-PDLLA micelles and Taxol micelles were investigated using transmission electron microscopy (JEM-1230 Electron

microscope, JEOL, Japan). To prepare samples, a dilute suspension of the micelles was dropped on copper grids, negatively stained with 1% (*w*/*v*) uranyl acetate, and allowed to dry under an ambient atmosphere.

2.5. Determination of the CMC

The CMCs of mPEG−PDLLA and Cremophor EL were measured according to a previously reported method with minor modifications[33]. Briefly, a series of aqueous mPEG−PDLLA solutions with concentrations from 0.01 to 100 mg/L containing 2 μmol/L pyrene were prepared and then incubated at 37 °C overnight under mild shaking. Meanwhile, a series of aqueous Cremophor EL solutions with a concentration from 0.01 to 400 mg/L containing 2 μmol/L pyrene were prepared and then incubated at 37 °C overnight under mild shaking. The fluorescence intensity of the samples was measured by a fluorospectrophotometer with the excitation wavelength fixed at 372 nm, while the emission wavelengths were set to 333 and 339 nm. The CMC value was obtained from the transition point in the plot of the fluorescence intensity ratio, I_{339}/I_{333}, *versus* the logarithm of the amphiphile concentration.

2.6. In vitro fluorescence stability study

The stability of PM in water and plasma was assessed by measuring the fluorescence intensity of P2-encapsulated PM. In brief, 0.5 mL of P2-encapsulated PM was added to 9.5 mL of plasma and incubated at 37 °C under shaking at 100 rpm (HZ-9211KB air thermostatic shaker, Hualida Laboratory Equipment Co., Ltd., Taicang, China). Samples were withdrawn at time intervals after incubation, and the fluorescence intensity of the samples was immediately measured by a Cary Eclipse fluorospectrophotometer (Agilent, USA). In parallel, the fluorescent stability of PM solution diluted with the same volume of ultrapure water was also evaluated.

2.7. In vitro analysis of PTX by HPLC

The concentration of PTX encapsulated in micelles or release medium was determined by high-performance liquid chromatography (HPLC). A mixture of water and acetonitrile (45/55, *v*/*v*) was utilized as a mobile phase. The elution rate was 1.0 mL/min, with the detection wavelength set at 227 nm. The encapsulation efficiency (EE) and drug loading (DL) of PTX were calculated according to Eqs. (1) and (2):

$$\text{EE}\ (\%) = (\text{Amount of PTX encapsulated in micelles})/(\text{Theoretical amount of PTX encapsulated in micelles}) \times 100 \quad (1)$$

$$\text{DL}\ (\%) = (\text{Amount of PTX encapsulated in micelles})/(\text{Amount of PTX encapsulated in micelles} + \text{amount of amphiphiles in micelles}) \times 100 \quad (2)$$

2.8. Fluorescence-based quantification of polymeric micelles

The quantification of polymeric micelles in biological media (blood and plasma) was performed by measuring P2 fluorescence. Their concentrations, expressed as polymer equivalents, were determined based on a pre-established fluorescence−concentration linear standard curve. To construct the standard curve, rat blood or plasma samples containing predetermined concentrations of polymeric micelles (ranging from 15.6 to 2000 μg/mL) were prepared by diluting P2-labeled PTX-loaded mPEG-PDLLA micelles with fresh heparinized rat blood or rat plasma. Aliquots (100 μL) of these samples with graded micelle concentrations were transferred to a black 96-well plate for fluorescence measurement using the IVIS system, with excitation and emission filters set at 710 and 760 nm, respectively. For the particokinetic analysis, fluorescence measurements of experimental blood and plasma samples were conducted alongside the standardized samples under consistent imaging parameters to ensure comparability.

2.9. In vitro release of PTX

The *in vitro* PTX release profiles from mPEG-PDLLA polymeric micelles and Taxol were investigated in PBS (pH 7.4) containing 1 mol/L sodium salicylate as reported previously[28]. First, 0.5 mL of PTX-loaded polymeric micelles or Taxol (200 μg PTX) was sealed into dialysis bags (M_W cutoff = 12,000−14,000, Spectrum Laboratories, Inc., Rancho Dominguez, CA, USA), immersed in 40 mL of release media and incubated at 37 °C under mild shaking. At predetermined time points, 1 mL of the media was withdrawn before replenishment with fresh media. The PTX concentration in the samples was determined by HPLC as described above. Experiments were conducted in triplicate.

2.10. Pharmacokinetic and particokinetic studies

The pharmacokinetics and particokinetics of PTX-loaded mPEG-PDLLA micelles as well as Taxol were investigated by monitoring PTX and fluorescence simultaneously. Briefly, PTX-loaded fluorescently labeled mPEG-PDLLA micelles as well as Taxol were intravenously administered to rats at a PTX dose of 5 mg/kg and a P2 dose of approximately 30 μg/kg. At predetermined time points of 0.0042, 0.083, 0.25, 0.5, 1, 2, 4, 8, 12, 24, 36, and 48 h post administration, 250 μL of blood samples were collected from the eye socket. Throughout the pharmacokinetic study, the rats were continuously monitored, and appropriate fluid supplementation was provided to maintain physiological stability. No abnormal changes in behavior, or body condition were observed in all rats. Immediately after sampling, 100 μL of blood was taken for fluorescence measurement by the IVIS-Spectrum system, and then re-collected for centrifugation. The blood samples were centrifuged at 3000 rpm (MicroCL 17R high-speed centrifuge, Thermo Fisher Scientific, USA) for 5 min to separate the plasma. One hundred microliters of plasma were taken for fluorescence measurement by IVIS and collected for storage at −20 °C until analysis. To extract PTX from plasma samples, 1 mL of *tert*-butylmethyl ether was added to 100 μL of plasma containing 10 μL of DTX (10 μg/mL) as an internal standard. After vortexing for 5 min and subsequent centrifugation at 12,000×*g* for 10 min, the organic layer was collected and dried under mild nitrogen flow at 40 °C. The samples were then dissolved in 100 μL of a mixed solvent (acetonitrile/water = 80/20, *v*/*v*) and centrifuged at 12,000×*g* for 15 min. Supernatants were obtained for further analysis by LC−MS/MS.

2.11. In vivo analysis of PTX by LC−MS/MS

Quantification of PTX by LC−MS/MS was conducted according to our previous literature[24]. Chromatography was performed utilizing an Agilent 1200 HPLC system equipped with a C18 column

(2.1 mm × 10 mm, 3.5 μm, Agilent Eclipse, USA) at a temperature of 30 °C and a flow rate of 1.0 mL/min. A mixture of acetonitrile and water (80/20, *v*/*v*) containing 0.1% formic acid was utilized as the mobile phase, and 5 μL of sample was injected for analysis. Mass spectrometric detection was conducted on an AB 4000 Q TRAP TM triple quadrupole linear ion trap mass spectrometer (SCIEX, USA) in positive ionization mode (ESI). Detection of the ions was conducted in multiple reaction monitoring (MRM) mode by monitoring the transition of *m*/*z* 854.4 → 509.3 for PTX and 808.4 → 226.1 for DTX.

Pharmacokinetic parameters were calculated using the DAS (Drug and Statistics for Windows) software (version 2.0).

3. Results and discussion

PTX-loaded PMs were prepared using a thin-film dispersion method adapted from established procedures with minor modifications[7,27]. The near-infrared fluorophore P2 was co-loaded to enable PM particle tracking and quantification. Transmission electron microscopy confirmed the PMs as monodisperse spherical particles (Fig. 1A and B), with a *Z*-average size of 33.88 ± 0.58 nm and polydispersity index of 0.08 ± 0.01 (Fig. 1C). This size exceeds the ~24 nm reported for the commercial PM product Genexol-PM®[7,29,30], likely attributable to the longer hydrophobic block in our copolymer (2.5 k *vs.* Genexol-PM®'s 1.75 k). PTX loading was 8.42 ± 0.54% (*w*/*w*), lower than Genexol-PM®'s reported 15.9%[31]. Further increasing PTX loading significantly increased particle size (to 59.6 nm) and concurrently decreased encapsulation efficiency (to 78.45%) (Supporting Information Fig. S1). Consequently, formulation optimization to match Genexol-PM®'s properties was not pursued.

Cremophor EL micelles (Taxol-Ms), reconstituted from Taxol® concentrate by saline dilution, served as a control. Taxol-Ms exhibited a smaller size (13.08 ± 0.10 nm) and polydispersity index (0.05 ± 0.04), consistent with the low molecular weight of Cremophor EL. Fluorescent labeling was achieved by incorporating P2 during initial PM preparation. The low P2 loading (0.0625%, *w*/*w*) ensured negligible impact on physicochemical properties[32-35].

CMCs of $mPEG_{2k}$-$PDLLA_{2.5k}$ and Cremophor EL were determined fluorometrically using pyrene and the environment-sensitive probe P2[35]. Pyrene yielded CMCs of 0.64 μmol/L (0.95 μg/mL) for the copolymer and 1.45 μmol/L (3.51 μg/mL) for Cremophor EL (Supporting Information Fig. S2). Consistent but more accurate values, validated previously[35], were obtained with P2: 0.21 μmol/L (0.31 μg/mL) and 1.37 μmol/L (3.31 μg/mL), respectively (Fig. 1D and E). The exceptionally low CMC of $mPEG_{2k}$-$PDLLA_{2.5k}$ confers superior stability against dilution, supporting structural integrity maintenance[36,37].

In vitro PTX release from PMs in 1 mol/L sodium salicylate was sustained but faster than from Taxol-Ms (Fig. 1F). PMs exhibited a greater burst release (23% *vs.* Taxol-Ms' 12%), followed by sustained release over 24 h. The subsequent gradual decline in cumulative release likely reflects partial PTX degradation[38,39]. This faster initial release, despite the high structural stability of mPEG-PDLLA micelles, can be attributed to weaker noncovalent interactions between PTX and the relatively mobile PDLLA core, which facilitate rapid diffusion without micelle disassembly. In contrast, Taxol-Ms released PTX more slowly, with less than 80% cumulative release at 48 h, despite their relative higher CMC values. This indicates that Taxol-Ms showed stronger affinity for PTX molecules[28,40].

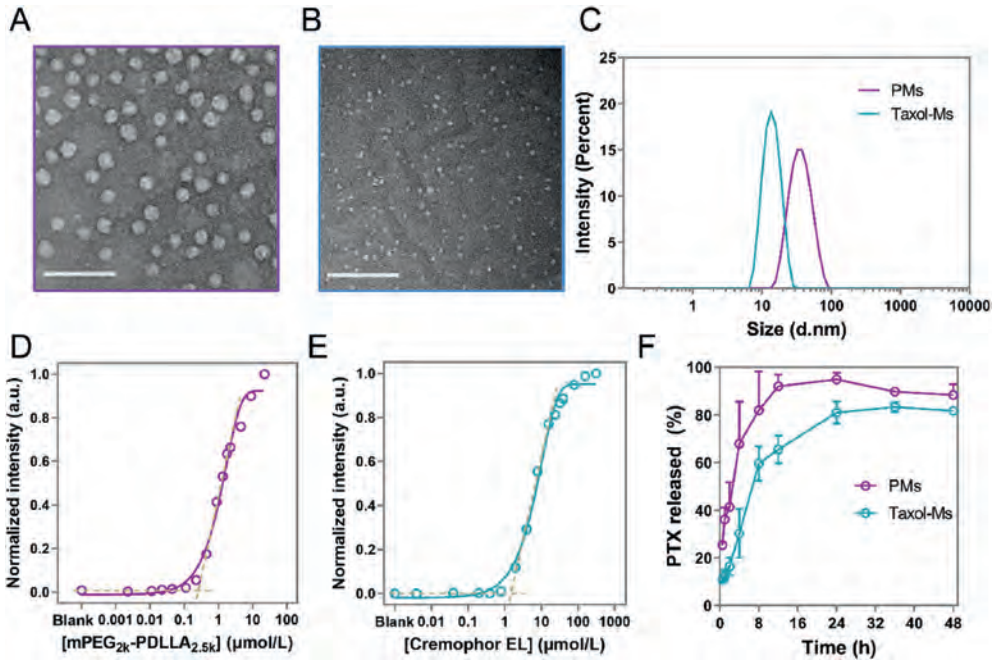

Figure 1 Characterization of P2-labeled PTX-loaded polymeric micelles (PMs) and Taxol-M. (A, B) TEM images of P2-labeled PTX-PMs (A) and Taxol-Ms (B). Scale bar, 100 nm. (C) Size distribution profiles of P2-labeled PTX-PMs and Taxol-Ms determined by dynamic light scattering. (D, E) The profiles of fluorescence intensity of P2 *vs.* the concentration of $mPEG_{2k}$-$PDLLA_{2.5k}$ (D) and Cremophor EL (E). The intercepts of the regression line of the linear regions with the *X*-axis indicate the CMCs of the copolymer and Cremophor EL. (F) *In vitro* PTX release profiles from PTX-PMs and Taxol-Ms. Data are presented as mean ± standard deviation ($n = 3$).

Accurate quantification of both PTX and PMs in biological samples like blood is essential for pharmacokinetic and particokinetic analysis. While established methods like HPLC/MS−MS enable precise PTX quantification[8,24], quantifying PMs presents a significant challenge due to difficulties in recovering intact particles from biological matrices. This study addressed the challenge by establishing a linear correlation between PM concentration and fluorescence intensity after labeling with the environmentally responsive near-infrared fluorophore P2.

Fig. 2A illustrates the principle for accurate PM tracking and quantification. Fluorophore P2 exhibits ACQ properties[32,41]. When encapsulated within the hydrophobic core of PMs, P2 fluoresces intensely. Conversely, unencapsulated or released P2 probes immediately aggregate upon aqueous contact, resulting in complete fluorescence quenching (intensity ≈ 0). This effectively eliminates interference from free probes, enabling specific quantification of intact PM vehicles[35,41-43].

Absorption and emission spectra of P2 in acetonitrile, P2-encapsulated PMs, and aqueous P2 dispersion confirmed labeling efficiency and probe water sensitivity. As shown in Fig. 2B−D, P2 in acetonitrile and PM-encapsulated P2 displayed strong near-infrared absorption and emission, while the

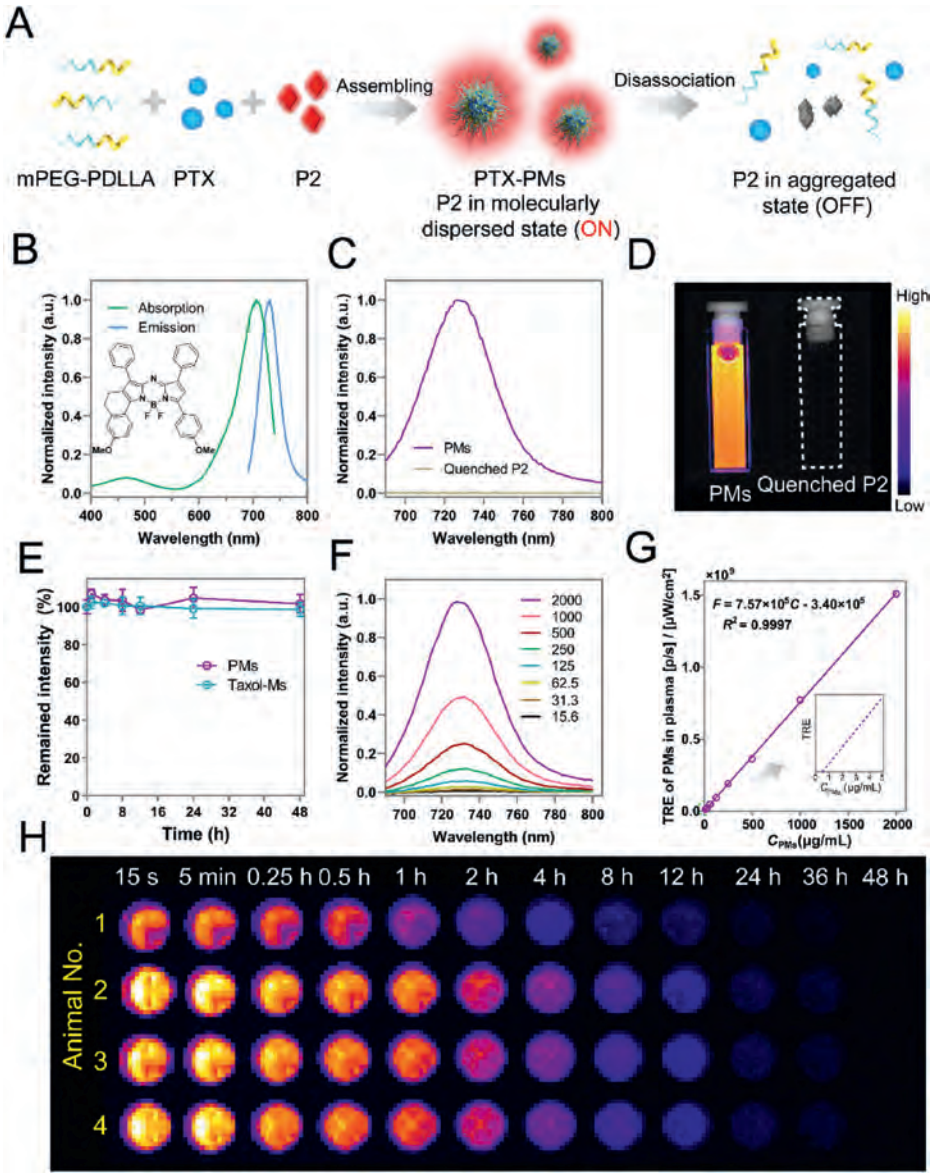

Figure 2 Spectroscopic and imaging studies of P2-labeled PTX-loaded polymeric micelles (PMs). (A) Rationale of imaging PMs following labeling by a NIR ACQ probe P2. (B) Absorption and emission spectra of P2 in acetonitrile. The inset shows the chemical structure of P2. (C, D) Emission spectra (C) and fluorescence images (D) of P2-labeled PMs in water and quenched P2 dispersion. Fluorescence images were captured by IVIS with excitation and emission wavelengths set to 710 and 760 nm, respectively. (E) Fluorescence stability profiles of P2-labeled PMs and Taxol-Ms in plasma. Data are presented as mean ± standard deviation ($n = 3$). (F) Fluorescence spectra of plasma samples doped with different levels (μg/mL) of P2-labeled PMs. (G) Linear correlation between P2 fluorescence (expressed as total radiance efficiency, TRE) monitored at the maximum emission of 760 nm and PM (expressed as the copolymer) concentration. (H) Well-plate fluorescence image of test plasma samples withdrawn at predetermined time points after intravenous administration of P2-labeled PMs to rats ($n = 4$).

aqueous dispersion was non-emissive due to ACQ. This ensures signals only originate from intact PMs, precluding interference from released P2 upon PM disassembly or degradation. P2 efficiently labeled both PMs and Taxol-Ms, and fluorescence signals remained stable for over 48 h in plasma (Fig. 2E), indicating maintained structural integrity.

To validate the fluorescence−PM concentration linearity, emission spectra and intensity of plasma spiked with varying P2-PM concentrations were measured. Plasma dilution reduced fluorescence intensity gradually while the emission maximum remained constant (Fig. 2F). Fluorescence intensity, measured by *in vivo* Imaging System (IVIS), showed excellent linear correlation ($R^2 = 0.9997$) with PM concentration (Fig. 2G). In contrast, PMs labeled *via* conventional Cy5.5 chemical conjugation exhibited poor linearity (Supporting Information Fig. S3)[44,45], confirming the superiority of the ACQ-based approach for PM quantification.

Notably, the linear regression for P2-PMs did not pass through the origin (Fig. 2G), intersecting the *x*-axis at a copolymer concentration of 0.45 μg/mL. This indicates complete PM disassembly below this concentration threshold. Remarkably, this critical disassembly concentration (0.45 μg/mL) was lower than the copolymer's CMC (0.95 μg/mL), highlighting the superior stability of PMs against dilution even in complex plasma[14,46]. In contrast, SMS micelles like Taxol-Ms showed greater sensitivity to plasma components, with a higher critical disassembly concentration (78 μg/mL, Supporting Information Fig. S4) than its CMC (3.51 μg/mL).

Based on the established linear correlations (Fig. 2G and Fig. S4), real-time quantification of PMs and Taxol-Ms in blood and plasma was achieved by directly measuring sample fluorescence using IVIS (Fig. 2H).

The particokinetics and pharmacokinetics of PTX-PMs were investigated and compared with those of Taxol-Ms following intravenous administration. The original and normalized particokinetic profiles for both micellar formulations in plasma and blood are presented in Supporting Information Fig. S5, Fig. 3A and B, respectively. PTX-PMs were cleared from the blood faster than Taxol-Ms over the 12-h period, except within the first 15 min. This accelerated clearance of PTX-PMs is likely attributable to their larger size, which promotes uptake and retention by the MPS[47,48]. Notably, within 5 min post-administration, the normalized concentration of PTX-PMs decreased from 100% to 91.55%, while that of Taxol-Ms decreased more markedly to 74.93% (Fig. 3A). This suggests that Taxol-Ms disassociate faster upon entering the circulation, corresponding to their higher CMC, indicative of lower stability compared to PTX-PMs.

Interestingly, Taxol-Ms subsequently demonstrated longer circulation times than PTX-PMs in plasma. Specifically, Taxol-Ms maintained higher plasma concentrations than PTX-PMs from 15 s to 12 h post-administration. The apparent inconsistency in Taxol-Ms clearance between blood and plasma within the initial 5 min may be due to the potent effects of Cremophor EL on erythrocytes, including inducing alterations in erythrocyte morphology, aggregation, hemolysis, and enhanced erythrocyte clearance[49-52]. Reduced uptake or attachment of Taxol-Ms to erythrocytes accounts for their high plasma/blood micellar ratio (Fig. 3C), which further diminishes erythrocyte uptake of the encapsulated drug payload[53,54]. The longer circulation time of Cremophor EL micelles enabled higher plasma PTX concentrations for Taxol-Ms compared to PTX-PMs for up to 24 h (Fig. 3D and E).

The faster clearance of PTX from PTX-PMs compared to Taxol-Ms is consistent with previous findings, which also reported a shorter plasma PTX half-life ($t_{1/2}$) for PTX-PMs (including mPEG-PDLLA micelles) than for Taxol-Ms[55-57]. Reduced erythrocyte uptake of PTX and the entrapment of PTX by circulating Cremophor EL micelles are widely considered the primary causes of this abnormal clearance pattern[53,54,58]. The pharmacokinetic profile of PTX-PMs resembled that of a PTX solution, indicating the complete and burst-like disassociation of PTX from the micelles upon entering the circulation. However, it remains unclear whether these results stem from rapid disassociation of the polymeric micelles themselves or rapid drug release.

To further elucidate the *in vivo* release behavior of PTX from PTX-PMs, we simultaneously measured plasma concentrations of the micellar particles and released PTX. The particokinetic profiles for the micelles and PTX (for both PTX-PMs and Taxol) are shown in Fig. 3F and G, Fig. S5, respectively. Compared to the micellar particles, the corresponding PTX was cleared much more rapidly from the circulation. For instance, within 5 min post-administration, approximately 10% of PTX-PMs were removed from plasma (Fig. 3A), while the plasma PTX concentration decreased by more than 90% (from 21.28 to 1.74 μg/mL) (Fig. 3E).

Fitting the data to a three-compartment model yielded the relevant pharmacokinetic and particokinetic parameters for PM particles and encapsulated PTX, respectively (Table 1). The distribution half-lives ($t_{1/2\alpha}$) and terminal elimination half-lives ($t_{1/2\gamma}$) of PTX were significantly smaller than those of the PM particles. This indicates that the elimination rate of PTX from the central compartment and the deep peripheral compartment was much faster than that of the intact micelles. Correspondingly, the elimination rate constant from the central compartment (K_{10}) and the distribution rate constants from the central to the shallow (K_{12}) and deep (K_{13}) peripheral compartments were significantly greater for PTX than for the PM particles. This demonstrates that PTX exhibits much faster clearance from the central compartment, as well as faster distribution to both peripheral compartments, than the intact micelles. A much greater K_{12} value compared to K_{10} and K_{13} for the PM particles indicates their rapid accumulation in shallow peripheral compartments (such as MPS organs), followed by slower redistribution to deep peripheral compartments. In contrast, a considerable proportion of PTX is either cleared directly from the central compartment or distributed to the deep peripheral compartment. These distinct kinetic behaviors provide further evidence that PTX is rapidly released from PTX-PMs and subsequently cleared *via* an independent pathway.

Although the comparison between pharmacokinetics and particokinetics reveals rapid release of PTX from the PM vehicles, calculating the exact release percentage at a specific time remains challenging. A schematic illustrates potential events occurring in the circulation following PTX-PMs entry into the blood stream (Fig. 4A). Initially ($t = 0$), all PTX is encapsulated within PM vehicles (initial PTX dose: D_0 or $(D_{PM})_0$, with inner subscript "$_{PM}$" indicating the PM-encapsulated form; initial PM dose: PM_0). At time t post-administration, several events may occur: 1) clearance of PMs from the blood and simultaneous distribution into various tissues/organs, reducing the total PM amount in the blood; 2) dissociation of PMs, releasing PTX and copolymer monomers; and 3) release of PTX from PMs without PM dissociation. Consequently, PTX may exist in either a PM-encapsulated form $(D_{PM})_t$ or free form $(D_F)_t$; the PM level at time t is described as PM_t.

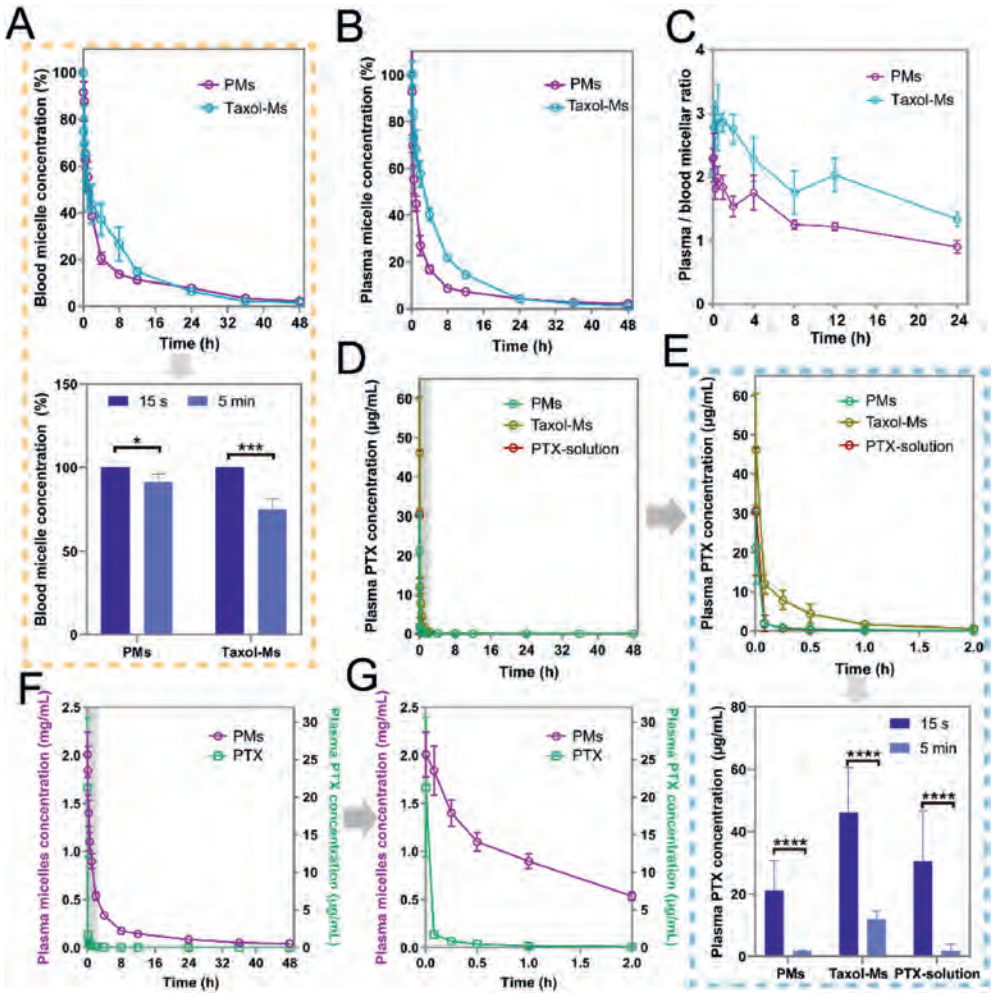

Figure 3 Simultaneous particokinetic and pharmacokinetic studies of PTX-loaded polymeric micelles (PMs) and Taxol-Ms. (A, B) Particokinetic profiles of PTX-PMs and Taxol-Ms in blood (A) and plasma (B) after administration to rats ($n = 4$). (C) Plotting the plasma/blood micelle ratio as a function of time after administration of PMs and Taxol to rats. (D) Pharmacokinetic profiles of plasma PTX after administration of PTX-PMs, Taxol, and PTX solution to rats at an equivalent PTX dosage of 5 mg/kg and (E) enlargement of plasma PTX *vs.* time profiles within the first 2 h and comparison of the data at 15 s and 5 min. (F) Plotting plasma micelles and PTX concentration as a function of time after administration of PTX-PM to rats and (G) enlargement of the profile within 2 h. Data are presented as mean ± standard deviation ($n = 4$). $^{*}P < 0.05$; $^{***}P < 0.001$; $^{****}P < 0.0001$, two-sided Student's *t* test.

Understanding strategies for profiling *in vitro* drug release can inform approaches to characterize *in vivo* release behavior. As noted in the introduction, two conventional methods exist for calculating drug release percentages: direct measurement of released ("free") drug in the bulk release medium, and quantification of residual drug within carriers followed by deduction from the initial dose. Conceptually, if the bloodstream were considered a closed release compartment with negligible drug loss from distribution or metabolism, *in vivo* release could be calculated by determining free drug concentration $(D_F)_t$ multiplied by blood volume. However, this approach proves impractical due to continuous extravascular biodistribution and poorly characterized drug metabolism. Similarly, the residual drug strategy requires carrier stability and recoverability—conditions unattainable for

Table 1 Particokinetic and pharmacokinetic parameters of plasma micelles and PTX after intravenous administration of PTX-PM to rats by fitting to a three-compartment model (mean ± SD, $n = 4$).

Formulation	$t_{1/2\alpha}$ (h)	$t_{1/2\beta}$ (h)	$t_{1/2\gamma}$ (h)	K_{10} (1/h)	K_{12} (1/h)	K_{21} (1/h)	K_{31} (1/h)	K_{13} (1/h)
PMs	0.29 ± 0.21	2.53 ± 1.82	27.98 ± 9.18	0.25 ±0.02	1.43 ±1.30	3.13 ±3.86	0.08 ±0.04	0.32 ±0.17
PTX	0.018 ± 0.002[a]	0.61 ± 0.13	13.04 ±0.78[a]	9.27 ±3.02[a]	18.51 ±1.64[a]	2.50 ±0.29	0.08 ± 0.08	8.60 ±2.67[a]

[a] $P < 0.05$.

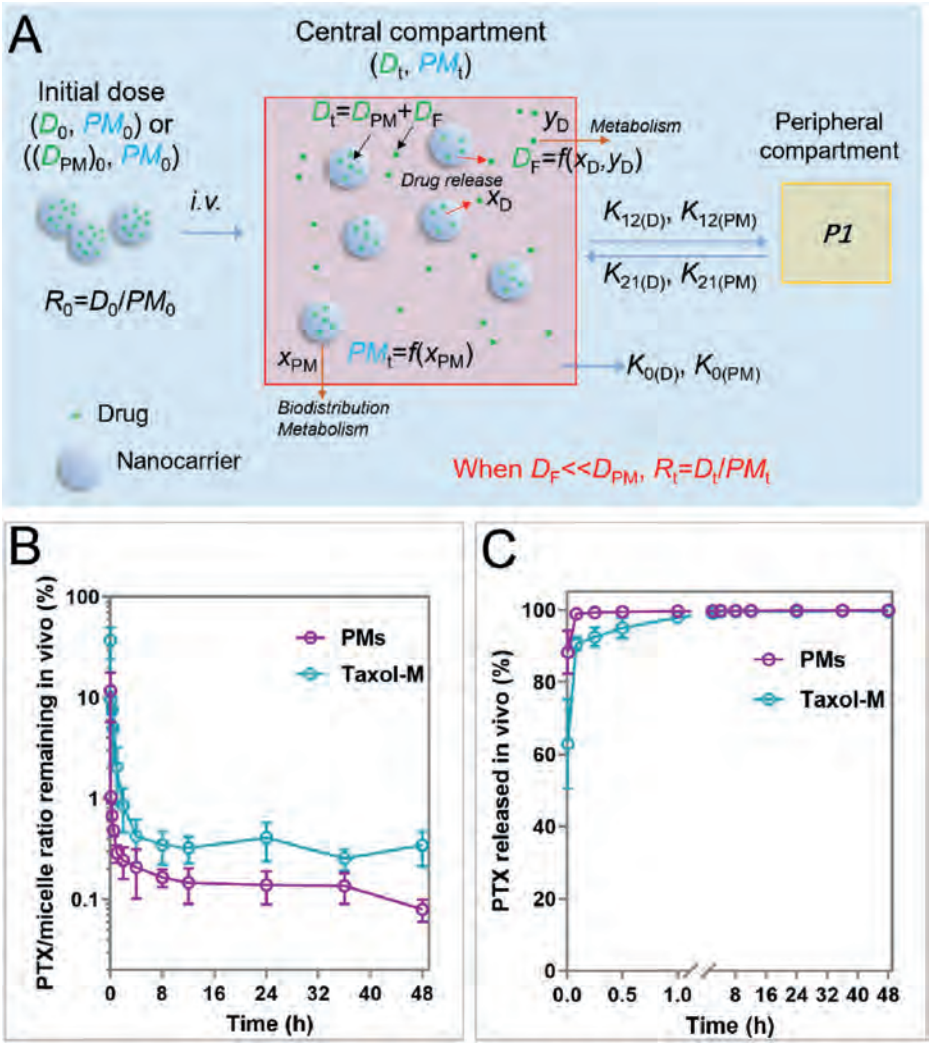

Figure 4 Schematic illustration of the *in vivo* fate of drug-loaded nanocarriers and profiling of the *in vivo* drug release kinetics. (A) Schematic illustration of events that may occur after i.v. administration of drug-loaded nanocarriers. (B) PTX/PM ratios calculated at different sampling time. (C) The *in vivo* release profiles of PTX from both PMs and Taxol calculated from dynamic change of PTX/PM ratios. Data are presented as mean ± standard deviation ($n = 4$).

multi-unit nanocarriers where confining particles within the vascular compartment and isolating carriers from biological matrices is impossible. The initial PM dose (PM_0) undergoes rapid blood clearance primarily *via* the MPS, while nanocarriers' small size and similarity to endogenous components preclude their separation from biological matrices.

In this study, we developed an alternative method to estimate *in vivo* release by tracking the drug-to-polymer mass ratio (R). This approach circumvents direct measurement of free or residual drugs and eliminates carrier separation requirements. The initial ratio ($R_0 = D_0/PM_0$, where D_0 is the initial drug mass and PM_0 the polymer mass) is readily determined from the drug loading data (Fig. 4A). At time t, the ratio R_t (defined as $(D_{PM})_t/PM_t$) represents encapsulated drug per polymer unit. While PM_t is measuable *via* our ACQ-based fluorescence method, $(D_{PM})_t$ cannot be directly assessed since total blood drug (D_t) comprises both encapsulated $(D_{PM})_t$ and free $(D_F)_t$ fractions. Accurate measurement of $(D_F)_t$ remains elusive due to drug leakage during conventional separation processes.

Critically, we observed rapid elimination of free PTX from the blood post i.v. administration, with $(D_F)_t$ constituting only a minor fraction of D_t at each sampling point. Upon entering the bloodstream, the fraction of released drug, $(D_F)_t$, is immediately cleared through fast plasma distribution. By contrast, the intact micelles follow a distinct particokinetic pathway characterized by slower clearance *via* long-circulating effect. The rapid divergence of the free-drug pathway from the micellar pathway results in only a negligible amount of freely circulating PTX at each sampling timepoint. This allowed approximation of $(D_F)_t \approx 0$ and therefore $R_t \approx D_t/PM_t$. A constant R_t/R_0 would indicate no release, but R_t decreased rapidly post-administration (Fig. 4B). At the first sampling time point (15 s), R_t dropped from approximately 1.08% to 0.095% within 5 min, stabilizing near 0.01%−0.02% after 4 h. Taxol-Ms showed a slower decline from 0.42% to 0.11% within 5 min, reaching approximately 0.05% by 4 h. These initial plasma ratios were markedly lower than formulation ratios (9.20% for PTX-PMs, 1.14% for Taxol-Ms), confirming immediate release upon blood contact. Converting R_t/R_0 to release percentage

(Fig. 4C) revealed PTX-PMs exhibited 88.24% burst release immediately post-injection, reaching 98.96% within 5 min, while Taxol-Ms showed 62.95% burst release with 90.61% within 5 min followed by gradual plateauing.

Notably, these profiles underestimate true *in vivo* release as measured plasma PTX (D_t) includes both encapsulated drug and residual free drug. The rapid plasma PTX decline primarily reflects release followed by immediate clearance, analogous to an *in vitro* dialysis system. This challenges the debated integrity of polymeric micelles *in vivo*[59,60]. While some propose drug-loaded PMs remain intact for targeted delivery[3,13,61,62], our data—using ACQ-labeled PMs with simultaneous particle/drug quantification—support evidence of rapid drug disassociation[11,44,56,63]. Several mechanisms have been proposed for this rapid drug release. Firstly, plasma proteins (*e.g.*, albumin) possess strong hydrophobic binding domains capable of competitively extracting PTX from the micellar core, thereby accelerating dissociation[64,65]. Secondly, the glass transition temperature (T_g) of PDLLA is close to physiological temperature (37 °C), likely increasing core chain mobility and facilitating PTX diffusion[66,67]. Thirdly, the constant high shear stress present in blood vessels may accelerate the repartition of PTX molecules[68,69]. The specific contributions of these mechanisms driving instant release warrant further investigation. Collectively, these findings not only suggest mPEG-PDLLA micelles primarily function as formulation "solvents" solubilizing hydrophobic PTX[70], rather than stable drug delivery vehicles, but underscore an alternative methodology for profiling the *in vivo* drug release of various nanoparticulate drug delivery systems with hydrophobic cores (*e.g.*, lipid nanoparticles and polymeric nanoparticles).

4. Conclusions

This study conclusively demonstrates that PTX is released with surprising rapidity from mPEG-PDLLA polymeric micelles *in vivo*, with over 88% released within 15 s and 99% within 5 min post-IV administration. By comparing PTX pharmacokinetics with PM particokinetics using a novel ACQ-fluorophore-based tracking method, the significant divergence revealed that the micelles function primarily as a solubilizing "solvent" rather than as stable, targeted delivery vehicles. This challenges the conventional view of PMs as long-circulating carriers and underscores the critical need to reassess their *in vivo* release behavior and true therapeutic mechanism for effective clinical translation.

Acknowledgment

This study was supported by the National Natural Science Foundation of China (No. 82030107).

Author contributions

Haisheng He: methodology, formal analysis, investigation, data curation, writing-original draft, visualization; Jianping Qi: resources, project administration; Yi Lu: resources, supervision, project administration; Wei Wu: conceptualization, methodology, writing-review & editing, visualization, supervision, project administration, funding acquisition.

Conflicts of interest

The authors declare no conflicts of interest.

Appendix A. Supporting information

Supporting information to this article can be found online at https://doi.org/10.1016/j.apsb.2025.11.034.

References

1. Cabral H, Miyata K, Osada K, Kataoka K. Block copolymer micelles in nanomedicine applications. *Chem Rev* 2018;**118**:6844–92.
2. Deshmukh AS, Chauhan PN, Noolvi MN, Chaturvedi K, Ganguly K, Shukla SS, et al. Polymeric micelles: basic research to clinical practice. *Int J Pharm* 2017;**532**:249–68.
3. Hwang D, Ramsey JD, Kabanov AV. Polymeric micelles for the delivery of poorly soluble drugs: from nanoformulation to clinical approval. *Adv Drug Deliv Rev* 2020;**156**:80–118.
4. Xie B, Liu Y, Li X, Yang P, He W. Solubilization techniques used for poorly water-soluble drugs. *Acta Pharm Sin B* 2024;**14**:4683–716.
5. Zhou Z, Li K, Chu Y, Li C, Zhang T, Liu P, et al. ROS-removing nanomedicine for navigating inflammatory microenvironment to enhance anti-epileptic therapy. *Acta Pharm Sin B* 2023;**13**:1246–61.
6. Shi H, van Steenbergen MJ, Lou B, Liu Y, Hennink WE, Kok RJ. Folate decorated polymeric micelles for targeted delivery of the kinase inhibitor dactolisib to cancer cells. *Int J Pharm* 2020;**582**:119305.
7. He H, Wang L, Ma Y, Yang Y, Lv Y, Zhang Z, et al. The biological fate of orally administered mPEG-PDLLA polymeric micelles. *J Control Release* 2020;**327**:725–36.
8. Awad R, Avital A, Sosnik A. Polymeric nanocarriers for nose-to-brain drug delivery in neurodegenerative diseases and neurodevelopmental disorders. *Acta Pharm Sin B* 2023;**13**:1866–86.
9. Liu Y, Fens MHAM, Capomaccio RB, Mehn D, Scrivano L, Kok RJ, et al. Correlation between *in vitro* stability and pharmacokinetics of poly (epsilon-caprolactone)-based micelles loaded with a photosensitizer. *J Control Release* 2020;**328**:942–51.
10. Haider MS, Lübtow MM, Endres S, Forster S, Flegler VJ, Böttcher B, et al. Think beyond the core: impact of the hydrophilic corona on drug solubilization using polymer micelles. *ACS Appl Mater Interfaces* 2020;**12**:24531–43.
11. Langridge TD, Gemeinhart RA. Toward understanding polymer micelle stability: density ultracentrifugation offers insight into polymer micelle stability in human fluids. *J Control Release* 2020;**319**:157–67.
12. Zhao X, Poon Z, Engler AC, Bonner DK, Hammond PT. Enhanced stability of polymeric micelles based on postfunctionalized poly(ethylene glycol)-*b*-poly(gamma-propargyl L-glutamate): the substituent effect. *Biomacromolecules* 2012;**13**:1315–22.
13. Su H, Wang F, Ran W, Zhang W, Dai W, Wang H, et al. The role of critical micellization concentration in efficacy and toxicity of supramolecular polymers. *Proc Natl Acad Sci U S A* 2020;**117**:4518–26.
14. Cai Y, Qi J, Lu Y, He H, Wu W. The *in vivo* fate of polymeric micelles. *Adv Drug Deliv Rev* 2022;**188**:114463.
15. Sarkar K, Torregrossa-Allen SE, Elzey BD, Narayanan S, Langer MP, Durm GA, et al. Effect of paclitaxel stereochemistry on X-ray-triggered release of paclitaxel from $CaWO_4$/paclitaxel-coloaded PEG-PLA nanoparticles. *Mol Pharm* 2022;**19**:2776–94.
16. Barkat MA, Beg S, Pottoo FH, Ahmad FJ. Nanopaclitaxel therapy: an evidence based review on the battle for next-generation formulation challenges. *Nanomedicine* 2019;**14**:1323–41.
17. Bernabeu E, Cagel M, Lagomarsino E, Moretton M, Chiappetta DA. Paclitaxel: what has been done and the challenges remain ahead. *Int J Pharm* 2017;**526**:474–95.
18. Sofias AM, Dunne M, Storm G, Allen C. The battle of "nano" paclitaxel. *Adv Drug Deliv Rev* 2017;**122**:20–30.

19. Bisso S, Leroux JC. Nanopharmaceuticals: a focus on their clinical translatability. *Int J Pharm* 2020;**578**:119098.
20. Cabral H, Kataoka K. Progress of drug-loaded polymeric micelles into clinical studies. *J Control Release* 2014;**190**:465−76.
21. Danhier F, Danhier P, De Saedeleer CJ, Fruytier AC, Schleich N, des Rieux A, et al. Paclitaxel-loaded micelles enhance transvascular permeability and retention of nanomedicines in tumors. *Int J Pharm* 2015;**479**:399−407.
22. Kim D, Le QV, Kim YB, Oh YK. Safety and photochemotherapeutic application of poly(gamma-glutamic acid)-based biopolymeric nanoparticle. *Acta Pharm Sin B* 2019;**9**:565−74.
23. Sheybanifard M, Beztsinna N, Bagheri M, Buhl EM, Bresseleers J, Varela-Moreira A, et al. Systematic evaluation of design features enables efficient selection of Π electron-stabilized polymeric micelles. *Int J Pharm* 2020;**584**:119409.
24. He H, Jiang S, Xie Y, Lu Y, Qi J, Dong X, et al. Reassessment of long circulation *via* monitoring of integral polymeric nanoparticles justifies a more accurate understanding. *Nanoscale Horiz* 2018;**3**:397−407.
25. Carstens MG, de Jong PH, van Nostrum CF, Kemmink J, Verrijk R, de Leede LG, et al. The effect of core composition in biodegradable oligomeric micelles as taxane formulations. *Eur J Pharm Biopharm* 2008;**68**:596−606.
26. Zhao W, Carreira EM. Conformationally restricted aza-bodipy: a highly fluorescent, stable, near-infrared-absorbing dye. *Angew Chem Int Ed* 2005;**44**:1677−9.
27. He H, Zhang J, Xie Y, Lu Y, Qi J, Ahmad E, et al. Bioimaging of intravenous polymeric micelles based on discrimination of integral particles using an environment-responsive probe. *Mol Pharm* 2016;**13**:4013−9.
28. Knemeyer I, Wientjes MG, Au JL. Cremophor reduces paclitaxel penetration into bladder wall during intravesical treatment. *Cancer Chemother Pharmacol* 1999;**44**:241−8.
29. Werner ME, Cummings ND, Sethi M, Wang EC, Sukumar R, Moore DT, et al. Preclinical evaluation of Genexol-PM, a nanoparticle formulation of paclitaxel, as a novel radiosensitizer for the treatment of non-small cell lung cancer. *Int J Radiat Oncol* 2013;**86**:463−8.
30. Lee SW, Yun MH, Jeong SW, In CH, Kim JY, Seo MH, et al. Development of docetaxel-loaded intravenous formulation, Nanoxel-PM™ using polymer-based delivery system. *J Control Release* 2011;**155**:262−71.
31. Gupta A, Costa AP, Xu X, Burgess DJ. Continuous processing of paclitaxel polymeric micelles. *Int J Pharm* 2021;**607**:120946.
32. Hu X, Zhang J, Yu Z, Xie Y, He H, Qi J, et al. Environment-responsive aza-BODIPY dyes quenching in water as potential probes to visualize the *in vivo* fate of lipid-based nanocarriers. *Nanomedicine* 2015;**11**:1939−48.
33. Yang Y, Lv Y, Shen C, Shi T, He H, Qi J, et al. *In vivo* dissolution of poorly water-soluble drugs: proof of concept based on fluorescence bioimaging. *Acta Pharm Sin B* 2021;**11**:1056−68.
34. Xia F, Chen Z, Zhu Q, Qi J, Dong X, Zhao W, et al. Gastrointestinal lipolysis and *trans*-epithelial transport of SMEDDS *via* oral route. *Acta Pharm Sin B* 2021;**11**:1010−20.
35. He H, Liu C, Lv Y, Qi J, Lu Y, Dong X, et al. Accurate and sensitive probing of onset of micellization based on absolute aggregation-caused quenching effect. *Aggregate* 2022;**3**:e163.
36. Zhang S, Zheng F, Liu K, Liu S, Xiao T, Zhu Y, et al. Mitochondria-targeting polymer micelles in stepwise response releasing gemcitabine and destroying the mitochondria and nucleus for combined antitumor chemotherapy. *Int J Mol Sci* 2022;**23**:12624.
37. Qiao Y, Zhan C, Wang C, Shi X, Yang J, He X, et al. MMP-2 sensitive poly(malic acid) micelles stabilized by pi−pi stacking enable high drug loading capacity. *J Mater Chem B* 2020;**8**:8527−35.
38. Kim S, Kim JY, Huh KM, Acharya G, Park K. Hydrotropic polymer micelles containing acrylic acid moieties for oral delivery of paclitaxel. *J Control Release* 2008;**132**:222−9.
39. Cho YW, Lee J, Lee SC, Huh KM, Park K. Hydrotropic agents for study of *in vitro* paclitaxel release from polymeric micelles. *J Control Release* 2004;**97**:249−57.
40. Brouwer E, Verweij J, De Bruijn P, Loos WJ, Pillay M, Buijs D, et al. Measurement of fraction unbound paclitaxel in human plasma. *Drug Metab Dispos* 2000;**28**:1141−5.
41. Qi J, Hu X, Dong X, Lu Y, Lu H, Zhao W, et al. Towards more accurate bioimaging of drug nanocarriers: turning aggregation-caused quenching into a useful tool. *Adv Drug Deliv Rev* 2019;**143**:206−25.
42. Cai Y, Ji X, Zhang Y, Liu C, Zhang Z, Lv Y, et al. Near-infrared fluorophores with absolute aggregation-caused quenching and negligible fluorescence re-illumination for *in vivo* bioimaging of nanocarriers. *Aggregate* 2023;**4**:e277.
43. Yuan H, Zhao W, Wu W. How can ACQ-based bioimaging of drug nanocarriers be improved?. *Ther Deliv* 2020;**11**:809−12.
44. Sun X, Wang G, Zhang H, Hu S, Liu X, Tang J, et al. The blood clearance kinetics and pathway of polymeric micelles in cancer drug delivery. *ACS Nano* 2018;**12**:6179−92.
45. Sun P, Wu Z, Xiao Y, Wu H, Di Q, Zhao X, et al. TfR-T12 short peptide and pH sensitive cell transmembrane peptide modified nanocomposite micelles for glioma treatment *via* remodeling tumor microenvironment. *Nanomedicine* 2022;**41**:102516.
46. Zuo R, Zhang J, Song X, Hu S, Gao X, Wang J, et al. Encapsulating halofuginone hydrobromide in TPGS polymeric micelles enhances efficacy against triple-negative breast cancer cells. *Int J Nanomed* 2021;**16**:1587−600.
47. Zhao Z, Ukidve A, Krishnan V, Mitragotri S. Effect of physicochemical and surface properties on *in vivo* fate of drug nanocarriers. *Adv Drug Deliv Rev* 2019;**143**:3−21.
48. Fan W, Peng H, Yu Z, Wang L, He H, Ma Y, et al. The long-circulating effect of pegylated nanoparticles revisited *via* simultaneous monitoring of both the drug payloads and nanocarriers. *Acta Pharm Sin B* 2022;**12**:2479−93.
49. Loos WJ, Szebeni J, ten Tije AJ, Verweij J, van Zomeren DM, Chung KN, et al. Preclinical evaluation of alternative pharmaceutical delivery vehicles for paclitaxel. *Anti Cancer Drugs* 2002;**13**:767−75.
50. Shimomura T, Fujiwara H, Ikawa S, Kigawa J, Terakawa N. Effects of Taxol on blood cells. *Lancet* 1998;**352**:541−2.
51. Zhang X, Liang N, Gong X, Kawashima Y, Cui F, Sun S. Tumor-targeting micelles based on folic acid and alpha-tocopherol succinate conjugated hyaluronic acid for paclitaxel delivery. *Colloids Surf B Biointerfaces* 2019;**177**:11−8.
52. Vader P, Fens MH, Sachini N, van Oirschot BA, Andringa G, Egberts AC, et al. Taxol®-induced phosphatidylserine exposure and microvesicle formation in red blood cells is mediated by its vehicle Cremophor® EL. *Nanomedicine* 2013;**8**:1127−35.
53. Sparreboom A, van Zuylen L, Brouwer E, Loos WJ, de Bruijn P, Gelderblom H, et al. Cremophor EL-mediated alteration of paclitaxel distribution in human blood: clinical pharmacokinetic implications. *Cancer Res* 1999;**59**:1454−7.
54. Jin M, Shimada T, Yokogawa K, Nomura M, Mizuhara Y, Furukawa H, et al. Cremophor EL releases cyclosporin A adsorbed on blood cells and blood vessels, and increases apparent plasma concentration of cyclosporin A. *Int J Pharm* 2005;**293**:137−44.
55. Kim SC, Kim DW, Shim YH, Bang JS, Oh HS, Wan Kim S, et al. *In vivo* evaluation of polymeric micellar paclitaxel formulation: toxicity and efficacy. *J Control Release* 2001;**72**:191−202.
56. Letchford K, Burt HM. Copolymer micelles and nanospheres with different *in vitro* stability demonstrate similar paclitaxel pharmacokinetics. *Mol Pharm* 2012;**9**:248−60.
57. Nakamura I, Ichimura E, Goda R, Hayashi H, Mashiba H, Nagai D, et al. An *in vivo* mechanism for the reduced peripheral neurotoxicity of NK105: a paclitaxel-incorporating polymeric micellar nanoparticle formulation. *Int J Nanomed* 2017;**12**:1293−304.
58. van Tellingen O, Huizing MT, Panday VR, Schellens JH, Nooijen WJ, Beijnen JH. Cremophor EL causes (pseudo-) non-linear pharmacokinetics of paclitaxel in patients. *Br J Cancer* 1999;**81**:330−5.
59. Owen SC, Chan DPY, Shoichet MS. Polymeric micelle stability. *Nano Today* 2012;**7**:53−65.
60. Ghezzi M, Pescina S, Padula C, Santi P, Del Favero E, Cantù L, et al. Polymeric micelles in drug delivery: an insight of the techniques for

their characterization and assessment in biorelevant conditions. *J Control Release* 2021;**332**:312−36.
61. Ghosh B, Biswas S. Polymeric micelles in cancer therapy: state of the art. *J Control Release* 2021;**332**:127−47.
62. Zhang H, Li H, Cao Z, Du J, Yan L, Wang J. Investigation of the *in vivo* integrity of polymeric micelles *via* large Stokes shift fluorophore-based FRET. *J Control Release* 2020;**324**:47−54.
63. Chen H, Kim S, He W, Wang H, Low PS, Park K, et al. Fast release of lipophilic agents from circulating PEG-PDLLA micelles revealed by *in vivo* Forster resonance energy transfer imaging. *Langmuir* 2008;**24**: 5213−7.
64. Liu J, Zeng F, Allen C. Influence of serum protein on polycarbonate-based copolymer micelles as a delivery system for a hydrophobic anti-cancer agent. *J Control Release* 2005;**103**:481−97.
65. de Oliveira MA, Pound-Lana G, Capelari-Oliveira P, Pontífice TG, Silva SED, Machado MGC, et al. Release, transfer and partition of fluorescent dyes from polymeric nanocarriers to serum proteins monitored by asymmetric flow field-flow fractionation. *J Chromatogr A* 2021;**1641**:461959.
66. Yamamoto Y, Yasugi K, Harada A, Nagasaki Y, Kataoba K. Temperature-related change in the properties relevant to drug delivery of poly (ethylene glycol)−poly (D,L-lactide) block copolymer micelles in aqueous milieu. *J Control Release* 2002;**82**:359−71.
67. Duran T, Costa A, Gupta A, Xu X, Zhang H, Burgess D, et al. Coarse-grained molecular dynamics simulations of paclitaxel-loaded polymeric micelles. *Mol Pharm* 2022;**19**:1117−34.
68. Feiner-Gracia N, Glinkowska Mares A, Buzhor M, Rodriguez-Trujillo R, Samitier Marti J, Amir RJ, et al. Real-time ratiometric imaging of micelles assembly state in a microfluidic cancer-on-a-chip. *ACS Appl Bio Mater* 2021;**4**:669−81.
69. Zhang H, He Z, Fu C, Pan P, Zhu Y, Xu M, et al. Dissociation of polymeric micelle under hemodynamic shearing. *Nano Today* 2022;**45**:101517.
70. Park K. Facing the truth about nanotechnology in drug delivery. *ACS Nano* 2013;**7**:7442−7.